ministerie van verkeer en waterstaat

koninklijk nederlands meteorologisch instituut

extension of the 3rd generation ocean wave model with refraction

Q.D. Gao

scientific reports WR 86-5

wetenschappelijke rapporten WR 86-5

de bilt 1986

KNMI

EXTENSION OF THE 3RD GENERATION OCEAN WAVE MODEL WITH REFRACTION.

Q.D. Gao.*

KNMI - De Bilt

1. Introduction

A so-called 3rd generation wave model has been developed with the purpose of having a reliable model for hindcast and of real time applications. S. and K. Hasselmann have presented a global version of the model and P. Janssen and G. Komen have extended this version to include certain shallow water effects. However, they did not take into account refraction due to variable bottom topography.
In this note, the extension of the shallow water model with refraction is described. In practice, refraction may be important in very shallow water because when coupled with shoaling, it leads to a wave energy redistribution in an uneven shallow water area, which can have a significant influence on wave height and direction.

* On leave of absence from Marine Environmental Forecasting Center, Beijing.

To treat refeaction we proceed as follows:

1. The total refraction is simply split into two terms; i.e. refractions due to a wave travelling along a great circle and refraction due to an incident wave moving at an angel with bottom contours.
2. Centered differentiation is adopted to calculate the bottom gradients in the finite difference grid.
3. An up-wind difference scheme is used to calculate the refraction.

We only consider here refraction due to variation of topography. Refraction caused by current, tide and other phenomena is considered negligible in this note.

The program of this note is as follows. We first describe in section 2 the energy balance equation for the frequency spectrum including refraction due to topography.

Next, in section 3 the numerical refraction scheme is presented and in section 4 the refraction scheme is tested for two idealized cases and one realistic hindcast of a major storm event on the European Continental Shelf in the beginning of January 1984.

2. Numerical Wave Model.

Following Hasselmann (1985), the evolution of the wave spectrum is described by the energy balance equation for the rate of change of the energy spectrum F, which is depentent on an source function S describing the energy gained or lost by each wave component. It reads in geographical coordinates:

$$\frac{\partial F}{\partial t} + \frac{\partial}{\partial \lambda}(\dot{\lambda}F) + \frac{\partial}{\partial \phi}(\dot{\phi}F) + \frac{\partial}{\partial \theta}(\dot{\theta}F) = S \qquad (1)$$

Here λ is longitude and ϕ latitude; $\dot{\lambda}$ and $\dot{\theta}$ are components of wave propagation angular speed along longitude and latitude respectively. θ is the wave propagation directon measured clockwise relative to the north in the usual navigation convention, $\dot{\theta}$ is split into two terms

$$\dot{\theta} = \dot{\theta}_1 + \dot{\theta}_2 \qquad (2)$$

where $\dot{\theta}_1$ is refraction due to wave travelling along great circle and $\dot{\theta}_2$ is refraction due to wave moving into variable topography area:

$$\dot{\theta}_1 = c_g \tan\phi \sin\theta/R, \tag{3a}$$

$$\dot{\theta}_2 = c_g \frac{\partial\theta}{\partial s} . \tag{3b}$$

Here R is the earth radius, s is distance along a wave ray and c_g is the wave group velocity

$$c_g = \tfrac{1}{2} (gk\tanh(k.d))^{\frac{1}{2}} \left(1 + \frac{2\,k.d}{\sinh(2k.d)}\right) ; \tag{4}$$

g is the gravitational acceleration, d is the water depth and the wave number k is determined by

$$\omega^2 = gk\tanh (k.d) . \tag{5}$$

Following Phillips (1977)

$$\frac{\partial\theta}{\partial s} = - (c_g k)^{-1} \left(- \frac{\partial d}{\partial x} \cos\theta + \frac{\partial d}{\partial y} \mathrm{Sin}\theta\right) \frac{\partial\omega}{\partial d}, \tag{6}$$

using $\frac{\partial\omega}{\partial d} = c_g \frac{\partial k}{\partial d}$ and for a given frequency

$$\frac{\partial k}{\partial d} = -k^2 . \mathrm{sech}^2(k.d)/(\tanh (k.d) + k.d\ \mathrm{sech}^2 (k.d)) ; \tag{7}$$

we obtain

$$\dot{\theta}_2 = \frac{c_g}{k} \left(- \frac{\partial d}{\partial x} \cos\theta + \frac{\partial d}{\partial y} \sin\theta\right) \frac{k^2 . \mathrm{sech}^2(k.d)}{(\tanh (k.d) + (k.d)\ \mathrm{sech}^2 (k.d))} . \tag{8}$$

3. Numerical Implementation of Refraction.

The rate of change of energy due to propagation effects is obtained in two steps. First, as in the deep water model, the energy change due to advection is calculated for each frequency bin and directional component. After that, refraction is added using a first-order, upwind, finite difference approximation (Golding)

$$\Delta F = \{\min (0, \dot{\theta}_2) F \big|_{\theta + \Delta\theta} + \max (0, \dot{\theta}_2) F\big|_{\theta - \Delta\theta} - \dot{\theta}_2 F\big|_{\theta} \} * \Delta t/\Delta\theta , \qquad (9)$$

where Δt is time interval for propagation, $\Delta\theta$ is angular resolution for discrete spectrum. In order to avoid instability, the condition $c_g \, \partial\theta/\partial s < \Delta\theta/\Delta t$ has to be imposed. It is easy to check that, in practice, this condition is satisfied for not too exotic bathymetries. As a precaution, for a single time step, the energy gained through refraction for each component is not allowed to exceed the modified Phillips saturation limit (Janssen and Komen)

$$\Delta F = 0.0005 \, \pi \, / \, c_g . \, k^3 . \qquad (10)$$

4. The test of Refraction calculation

The numerical refraction scheme described above has first been tested on two different idealized bottom topographies. In the first test, a parabolic sea mountain was considered, in the second a constant bottom slope. During the experiments, advection, refraction and dissipation due to wave breaking were retained in the model and non-linear interaction, wind-input and bottom friction were switched off. All runs were performed on a square grid with distance 50 km. The model was initialized to zero energy everywhere except along one boundary on which a constant energy flux was introduced by specifying a given energy at all time. At the other boundaries complete energy absorption was assumed.

Fig. 1 gives the steady solution obtained after swell crossed the sea

mountain. The propagation angle changes clockwise as the swell approaches the sea mountain, on the top of which there is a strong convergence of energy because of refraction coupling with shoaling. The energy divergence occurs between the deep and shallow water area where the angle between two adjacent swell crests increases as the swell moves forward.

Fig. 2 shows the constant bottom slope case where the incoming swell makes an angle of 45° with bottom contours. A comparison was made between the numerical results and analysis calculation based on Snell's law, which reads

$$\frac{\sin(\alpha_1)}{\sin(\alpha_2)} = \frac{c_1}{c_2} \,. \qquad (11)$$

Here α_1 is the incident angle of the swell in deep water and c_1 is its phase speed, α_2 is the angel measured at a position in shallow water; c_2 is the phase velocity at that position. The results of the comparison shown in table 1 are satisfactory.

The tests were performed on a Cray XMP/48 computer, 50 seconds CPU time were needed for 48 propagation time steps while 44 seconds were needed without refraction for the same number of time steps

The WAMS model as described by Janssen and Komen (1985) and Bertotti et al (1986) was extended by including a refraction subroutine. It was decided to test this software package on the major storm event on the European Continental Shelf in the period of 1-4 January 1984. The run was performed on a fine mesh grid (½ deg. longitude, ¼ deg. latitude) covering part of the North Atlantic, the Norwegian Sea and the North Sea (20° west to 10°east, and 50 to 70° north). The total number of grid points was about 4500. In order to prevent numerical instability of the first-order upwinding advection scheme an integration time step of 15 minutes was chosen. The grid is presented in fig. 3 and the bottom topography is given in fig. 4. In fig. 4 also the output points, where spectral information is available, in principle, are indicated.

Just as in the WAMS project (Bertotti et al) the warming up period of the model was taken to be two days.

Fig. 5 gives the time series for wave height at IJmuiden. For comparison also the time series for wave height obtained with the WAMS model without refraction is shown. Evidently, the effect of refraction is

small. We think that one of the main reasons for this is that owing to bottom friction the long wave are readily dissipated and since refracton has mainly an effect on long waves no big effect due to refraction is to be expected. Also, as shown in Table 2, the effect of refraction on the wave direction was very small.
The run with refraction took 10% more CPU time than the run without refraction.

5. Conclusion

A numerical refraction scheme has been tested on two idealized cases and implemented in the WAMS model. The scheme seems to work satisfactorily. In closing please note that although in our hindcast the effect of refraction was small (because of wind sea with high peak frequency) refraction may have a significant effect on low-frequency, swell trains, especially on its direction.

References.

Bertotti L., Guillaume, A. and Janssen P.(1985). The WAMS project, first test of a shallow water, third generation model against data.

Golding, B.W; (1983): A wave prediction system for real-time sea state forecasting. Q.J.R. Meteorol. Soc. 109. p. 393-417.

S. Hasselmann and K. Hasselmann (1985). A global wave model. Report; Max-Planck-Institut für Meteorologie, June 30, 1985.

Janssen P. and Komen G. (1985). A shallow water extension of the 36-WAM model. (Unpublished manuscript)

Phillips O. (1977). The dynamics of the upper Ocean.

depth (m)	results of numerical calculation	results of analytical solution	depth (m)	results of numerical calculation	results of analytical solution
∞	45°	45°	60	36°	35.5°
110	43°	43°	50	34.5°	33.5°
100	42°	41.5°	40	31°	30°
90°	41°	40.5°	30	28°	27°
80	39.5°	39.0°	20	25°	32°
70	38°	37.5°	10	21°	18°

Table 1. comparison between numerical calculation and analytical solution based on Snell's law. The angles are relative to the direction perpendiculat to the bottom slope.

IJmuiden Wave direction 2 153

Date	WAMS	WAMSR	Ø
84010100	73	75	60
03	77	78	68
06	82	84	74
09	81	84	60
12	72	74	59
15	67	69	54
18	65	67	53
21	69	71	68
84020200	76	77	77
03	91	93	100
06	105	107	94
09	112	115	80
12	112	117	52
15	80	89	20
18	43	44	22
21	45	45	38
84010300	48	49	40
03	55	57	45
06	67	70	85
09	80	81	87
12	77	79	67
15	76	76	72
18	85	87	95
21	93	96	91
84010400	101	102	95
03	108	110	101
06	123	126	136
09	139	142	151
12	145	148	145
15	150	152	149
18	155	158	145
21	161	165	144
84010500	162	166	125

Table 2: Effect of refraction (WAMSR) on the average wave direction. Here Ø is the local wind direction.

Figure Captions

Fig. 1 The single component (f = 0.04 Hz) moves over a parabolic sea mountain. The dashed lines are the sea bottom contours and the arrows indicate the propagation direction, the solid lines are swell height and the crosses x denote energy flux point where a constant energy flux is prescribed.

Fig. 2 Swell travelling over diagonal bottom contours with single frequency (f = 0.04 Hz). The meaning of crosses, dashed lines and arrows are as in Fig. 1.

Fig. 3 Grid of the limited area wave model WAMSR.

Fig. 4 Bottom topography of the limited area model.

Fig. 5 Time series of wave height at IJmuiden. Δ-Δ = no refraction;..... with refraction; ☐ are the measurements.

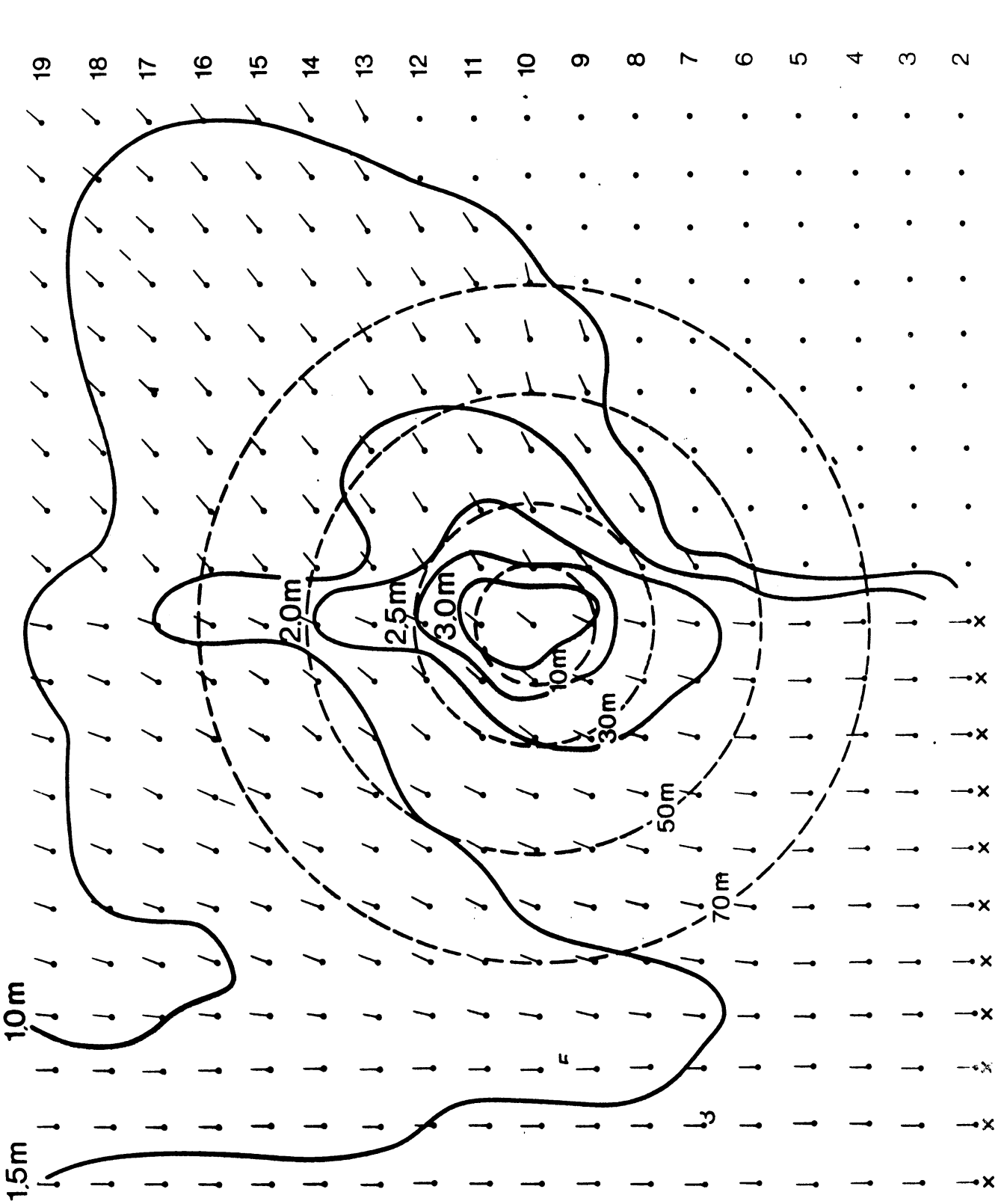
19
18
17
16
15
14
13
12
11
10
9
8
7
6
5
4
3
2
1.0m
1.5m
2.0m
2.5m
3.0m
10m
30m
50m
70m

Fig. 1

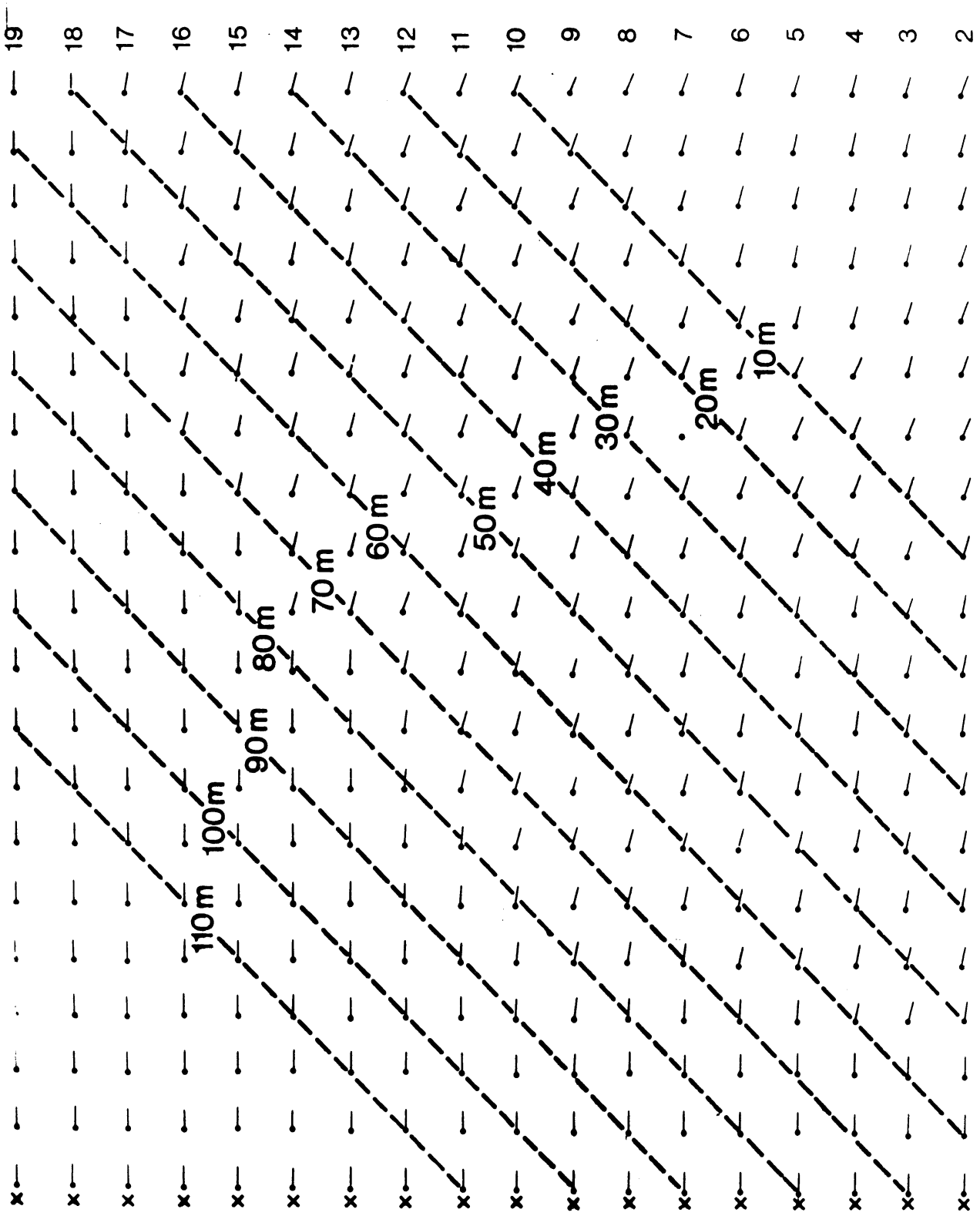
19
18
17
16
15
14
13
12
11
10
9
8
7
6
5
4
3
2
10m
20m
30m
40m
50m
60m
70m
80m
90m
100m
110m

Fig. 2

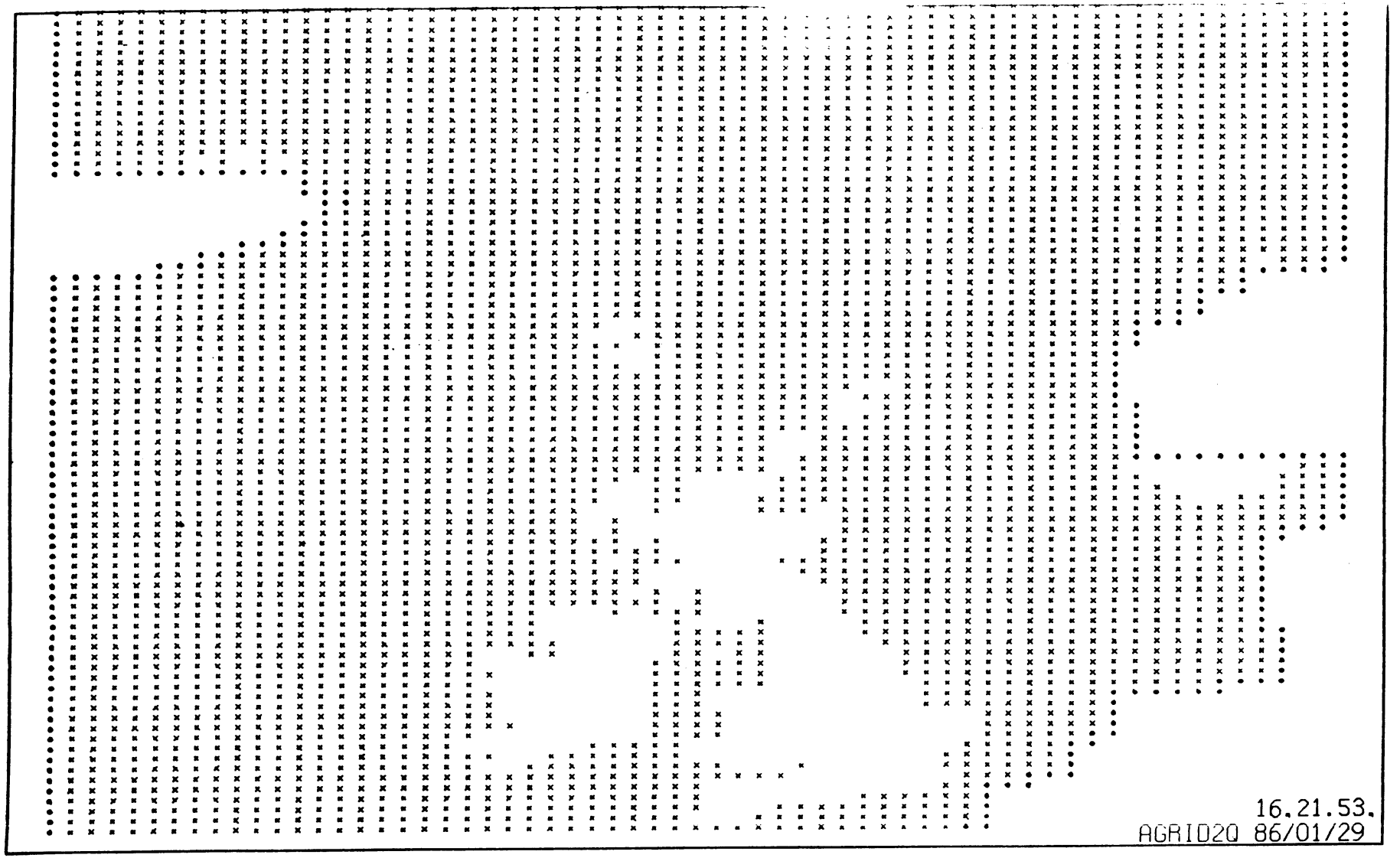

FIG. 3

FIG. 4 WAMS PROJECT FINE MESH GRID BATHYMETRY

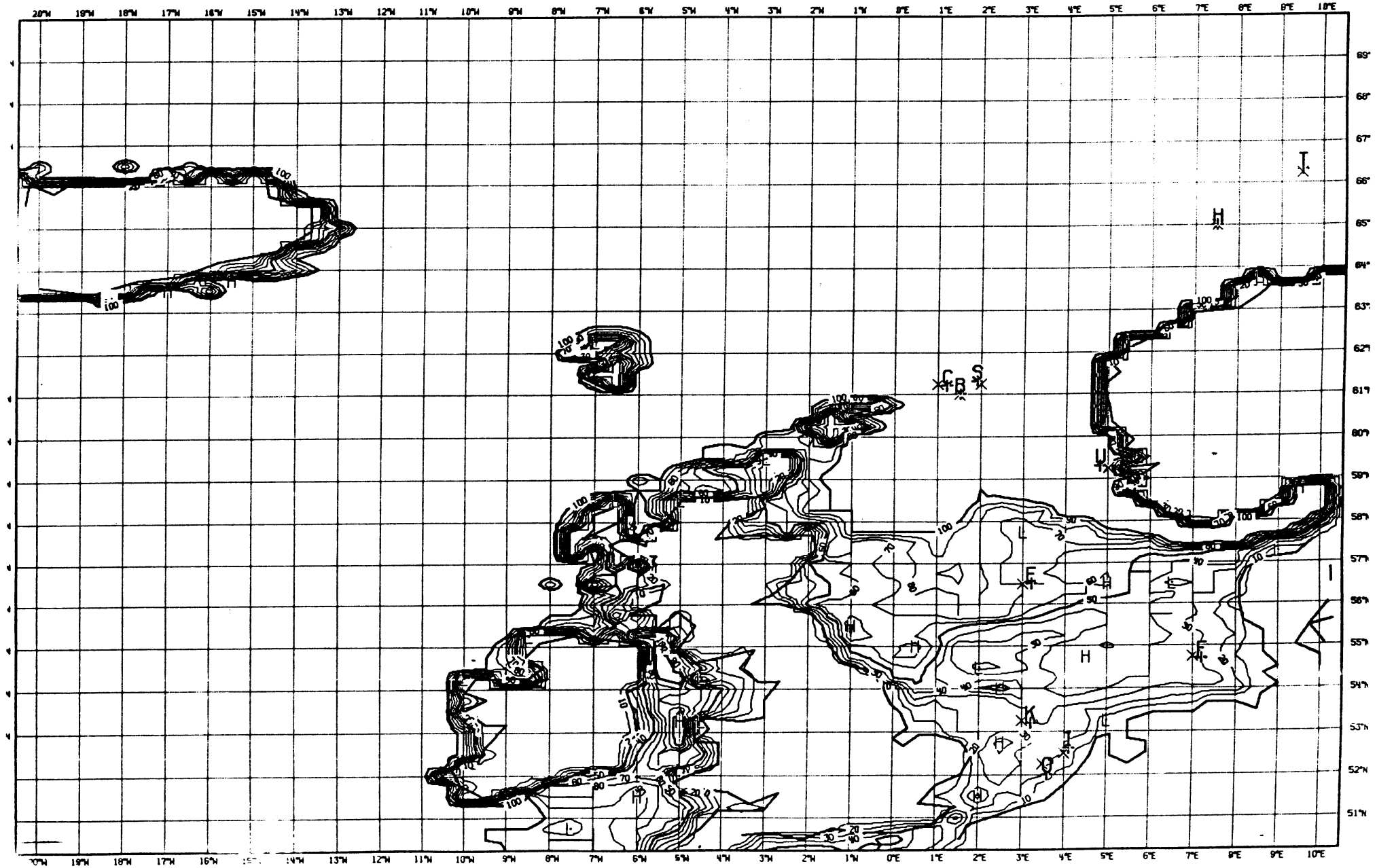

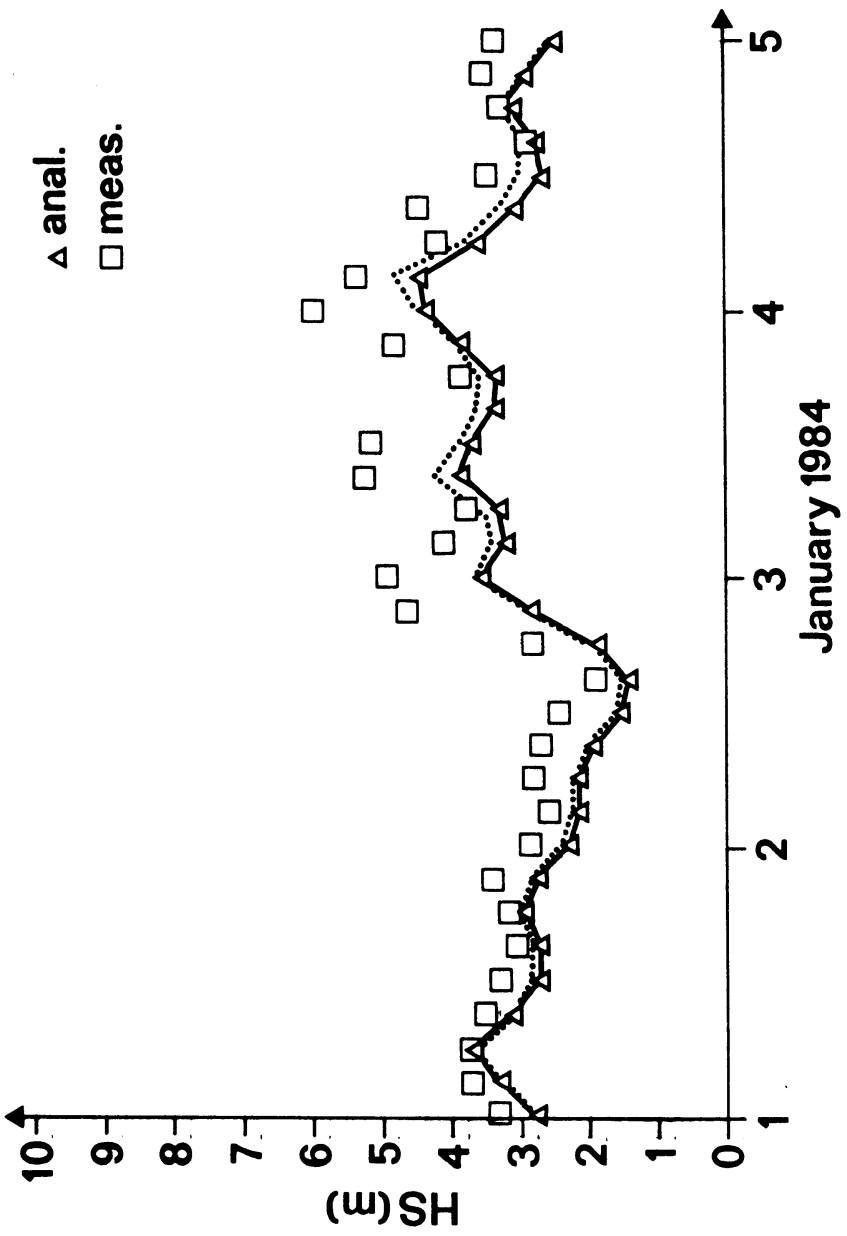

Fig. 5